applied sciences

MDPI

Article

Silver Nanoparticles-Loaded Exfoliated Graphite and Its Anti-Bacterial Performance

Shiyu Hou [1,2], Jihui Li [1], Xiaochuan Huang [3], Xiaomao Wang [3], Liqiang Ma [2], Wanci Shen [1], Feiyu Kang [1] and Zheng-Hong Huang [1,*]

1 State Key Laboratory of New Ceramics and Fine Processing, School of Materials Science and Engineering, Tsinghua University, Beijing 100084, China; 15201323501@163.com (S.H.); lijihuimail@sina.com (J.L.); shenwc@mail.tsinghua.edu.cn (W.S.); fykang@sz.tsinghua.edu.cn (F.K.)

2 School of Chemical and Environmental Engineering, China University of Mining and Technology (Beijing), Beijing 100083, China; mlqiang@sina.com

3 State Key Joint Laboratory of Environmental Simulation and Pollution Control, College of Environment, Tsinghua University, Beijing 100084, China; huangxc14@mails.tsinghua.edu.cn (X.H.); wangxiaomao@tsinghua.edu.cn (X.W.)

* Correspondence: zhhuang@mail.tsinghua.edu.cn; Tel.: +86-10-6277-3752; Fax: +86-10-6277-1160

Received: 11 July 2017; Accepted: 15 August 2017; Published: 18 August 2017

Abstract: One antibacterial material was prepared from exfoliated graphite (EG) decorated with silver nanoparticles (AgNPs). The EG was prepared by the graphite intercalated compound process, AgNPs were prepared by chemical reduction of $AgNO_3$ in the presence of $NaBH_4$. The AgNPs-loaded EG (Ag-EG) composite was characterized by X-ray diffraction (XRD), Fourier transform infrared spectroscopy (FT-IR), nitrogen adsorption, mercury intrusion porosimetry, scanning electron microscopy (SEM), and transmission electron microscopy (TEM). The antibacterial effect of the Ag-EG was evaluated by using the zone of inhibition method. The loaded AgNPs were highly dispersed on EG sheets and most of them have a size less than 10 nm. The Ag loading slightly increased the surface area of EG. It is shown that the Ag-EG had antibacterial activity and anti-adhesion properties against *Pseudomonas aeruginosa* and *Staphylococcus aureus*. It suggests that Ag-EG composites could be used in a variety of industrial applications that require an antibacterial effect.

Keywords: exfoliated graphite; GICs; Ag nanoparticles; Ag-EG composites; antibacterial activity; *Pseudomonas aeruginosa*

1. Introduction

Microbial pollution caused by microorganisms has produced various problems in daily life (wound infection) and industry (wastewater discharge). Silver metal and compounds exhibit robust wide-spectrum bactericidal activity compared to other metal materials [1–4]. Ag nanoparticles (AgNPs) are used in antimicrobial applications due to the antimicrobial effect of Ag ions. Nevertheless, practical applications of AgNPs may lose antibacterial activity owing to aggregation among particles [5,6]. An effective way to prevent AgNPs from aggregation is to deposit AgNPs on some supports to fabricate AgNPs-loaded materials. Silica nanowires [7–10], zeolite clay [6], titanium dioxide nanoparticles [11], and montmorillonite have been investigated for antibacterial support materials. However, unfavorable biocompatibility, large size, and low dispersity of these composites limit their practical applications.

With huge specific surface area, proper micropores and excellent adsorption capacity, porous carbon materials have been widely used in wastewater treatments [12] and antibacterial support materials. Silver-loaded activated carbons, silver-loaded activated carbon fibers (Ag-ACFs) [13–15], and silver-loaded carbon aerogels [16] not only keep the excellent adsorption capacity of porous

carbon materials, but also endow them with antibacterial activity. Nanocarbon materials such as carbon nanotubes (CNT) [17,18] and graphene [19–22] have also been investigated as silver-carrying antibacterial agents. Especially graphene, for AgNPs loading, is a favorable matrix because of their abundant functional groups and large surface areas. A work provides the first direct evidence that Ag-loaded graphene oxide (Ag-GO) nanocomposites can inhibit the growth of microbial adhered cells, thus preventing the process of biofilm formation [23]. Liu et al. [24] and Das et al. [25] demonstrated antibacterial activity for Ag-GO nanocomposites against Gram-negative *Escherichia coli*. The preparation of graphene is very complex and expensive; material availability and process-ability will encumber the performance and putative applications of graphene [26].

Exfoliated graphite (EG) has layered structures, possessing in-plane electrical conductivity similar to that of natural flake graphite, but has larger layer spacing and higher volume. EG can be mass-produced and used in many applications such as gaskets, seals, etc. EG has abundant pore structure and excellent adsorption performance, and thus can be potentially used in depollution. For example, EGs have been studied for usage in dyeing wastewater treatment [27,28]. EG has oxygen-containing functionalities such as hydroxyl, carboxylic, carbonyl, epoxide groups and can provide nucleation sites for Ag nanoparticles, therefore, Ag nanoparticles can strongly attach to the EG surface to obtain AgNPs-loaded EG. Compared to general polymer-based Ag composites [3], this material would have higher thermal and chemical stability. Ag-EG composite material keeps the electrical/thermal conductivity of EG, and its antibacterial effect gives it more extensive applications in industrial applications. Recently, metal nanoparticles-supported carbon materials have been effectively used for biomedical applications including wound healing [29,30]. EGs possess excellent adsorption ability for protein [31], thus Ag-EG composites could be used as surgical dressing.

In this study, we designed EG as the AgNPs' support, and prepared a new anti-bacterial composite. Firstly, graphite was chemically oxidized, and then was reduced by $NaBH_4$ together with $AgNO_3$ at normal atmospheric conditions. Finally, the antibacterial activities of Ag-EG composite materials were evaluated by using the zone of inhibition method.

2. Materials and Methods

2.1. Materials

Flake graphite (50 mesh), silver nitrite ($AgNO_3$, 99.7%, reagent grade), $NaBH_4$ (98%, reagent grade), sulfuric acid (laboratory reagent grade, assay $\geq$ 98%), hydrochloric acid (reagent grade, assay 37%), H_2O_2 (laboratory reagent grade, assay 29.0~32.0%, *w*/*w*), these reagents were purchased from Sigma Aldrich (Shanghai) Trading Co., Ltd. (Shanghai, China). Lysogeny broth (g/L, peptone 10 g, yeast extract 5 g, NaCl 10 g; agar powder 10 g, pH 7), phosphate buffer saline (g/L, NaCl 8 g, KCl 0.2 g, KH_2PO_4 0.24 g, Na_2HPO_4 1.44 g, pH 7) were purchased from Yocon biotechnology Co., Ltd. (Beijng, China).

2.2. Preparation of Graphite Intercalation Compounds (GICs)

GICs were prepared from flake graphite by a chemical oxidation method. Generally, 1 g of flake graphite was added to 6 mL of concentrated H_2SO_4 in an ice bath. 0.2 mL of 30% H_2O_2 solution was then added slowly with stirring, keeping the temperature of the reaction mixture below 5 °C. The temperature of the reaction mixture was increased and maintained at 40 °C for 1 h. The product was then filtered and washed with ultrapure water until pH was between 5 and 7. GICs was obtained after dried in an air-oven at 60 °C for 2 h.

2.3. Preparation of Ag Nanoparticles-Loaded Exfoliated Graphite

0.5 g GICs mixed with 70 mL $AgNO_3$ solution (3.125×10^{-4} mol·dm^{-3} to 8×10^{-2} mol·dm^{-3}). Then the reaction mixture was stirred for 1 h at room temperature before addition of the reducing agent. 2 mL of 0.01 mol·dm^{-3} freshly prepared solution of $NaBH_4$ was added slowly to the reaction

mixture of $AgNO_3$–GICs suspension under vigorous stirring. The reaction mixture was stirred for another 5 h for the complete reduction at room temperature. The product was then filtered and washed with ultrapure water until the filtrate cannot produce white precipitate with 10% hydrochloric acid. Ag-GICs were obtained after drying in an air-oven at 60 °C for 2 h. Eventually, Ag-GICs in a quartz beaker with scale were put into an electric muffle furnace by rapid heating at 950 °C for a few seconds, AgNPs-loaded EG was obtained until the volume of EG was not changed. We can observe the quartz beaker's scale to estimate the process of exfoliation.

2.4. Structural Characterization

The crystalline structure of Ag nanoparticles were characterized by X-ray diffraction (XRD, Rigaku D/max 2500 V, Target = Cu, Step width = 0.01, operating at an acceleration voltage of 40 kV). FT-IR of the EG and Ag-EG was performed by Bruker FT-IR spectrophotometer. Mixed EG and KBr were ground to powder, then compressed into thin slices. FTIR spectra were recorded with 4 cm^{-1} resolution over the range 500–4000 cm^{-1} using a Vertex 70 Fourier transform infrared spectrometer. Nitrogen adsorption–desorption measurement was performed to investigate the specific surface area (SSA) using a BEL–SORP–II (BEL Japan, Inc., Tokyo, Japan) system at 77 k, the SSA were calculated using the Bruauer–Emmett–Teller (BET) equation. The pore size distribution of EG and Ag-EG was measured by mercury intrusion porosimetry (Micromeritics, AutoPore IV 9500, from pressure 0.20 to 60,000.00 psia). The morphology of exfoliated graphite was observed by scanning electron microscopy (SEM, MERLIN Compact, Carl Zeiss, Jena, Germany), the samples were coated with a layer of sputtered gold using a vacuum sputter to provide electrical conductivity before SEM observation. At the same time, Energy Dispersive Spectrometer (EDS) was used to examine the nanoparticles loaded on the surface of EG. High-resolution transmission electron microscope (HR-TEM) images were obtained on a JEOL JEM-2100 F. Samples for HRTEM imaging were prepared by placing a drop of the solution sample (Ag-EG was suspended in ethyl alcohol and treated through ultrasonication for 2 h) onto a carbon-coated Cu grid, dried in air and loaded into the electron microscopic chamber. The Ag content was obtained by ICP-AES (VISTA-MPX, VARIN). The samples for ICP-AES were prepared as below: certain amount of Ag-EG and the mixture of HNO_3 and $HClO_4$ solution were put into digestion high-pressure tank, the nitrolysis process accomplished in an oven, then a metered volume of solution was obtained to be tested.

2.5. Antibacterial Activity and Anti-Adhesion Effect of Bacteria

The antibacterial activity of Ag-EG was studied against the Gram negative bacterial strain *Pseudomonas aeruginosa* (ATCC 10145) and Gram positive bacterial strain *Staphylococcus aureus* (ATCC 27217). The bacterial strains were grown in lysogeny broth (LB) at 37 °C with continuous shaking at 200 rpm for 12 h. Ten mL bacterial cultures were separated by centrifugation (5000 rpm, 4 °C), the supernatant was discarded, 10 mL PBS was added and shaken up, then the bacterial solution was separated by centrifugation, this step was repeated three times. Finally, a bacterial solution (approx. 10^9 CFU) without LB was obtained. A mixture of nutrient broth and nutrient agar in 1 L distilled water at pH 7.2 as well as the empty Petri plates were autoclaved, the agar medium was then cast into the Petri plates and cooled. Two to three mg Ag-EG were made into round pieces with diameter of 6 mm. 0.2 mL bacterial solution was homogeneously dispersed on solid medium, then the round piece was placed on the solid medium. The inhibition zone images were collected by a digital camera after 24 h incubation at 37 °C. Each Petri plate had four Ag-EG round pieces to reduce the error.

The anti-bacterial adhesion effect was also evaluated by the colony-counting method. The round pieces of EG and Ag-EG were sterilized by ultraviolet light, the *P. aeruginosa* and *S. aureus* bacterial strains were washed in PBS by the method mentioned above, then round pieces were incubated with washed bacteria for a couple of hours at 37 °C. The samples were washed by a combination of sonication and severe stirring to remove all loosely attached bacteria, then the round pieces were stamped on the solid medium. The bacterial communities were counted after 24 h incubation at 37 °C.

3. Results and Discussion

3.1. XRD and FTIR Analysis

To improve the synthesis of Ag-EG composite, a series of characterization techniques were applied. Figure 1a shows the X-ray diffraction (XRD) patterns of the graphite, GICs, and Ag-GICs. The (002) diffraction peak of graphite appears at 26.56°, GICs at 26.06°, the slight change in the location of the (002) diffraction peaks relative to graphite is ascribed to the oxygen-containing groups on the surface of GICs [32]. In the insert picture, the peaks at 38.1°, 44.4°, 64.5°, and 77.5° can be assigned to the (111), (200), (220), and (311) planes of silver with the face-centered cubic (fcc) structure (space group: Fm3m), respectively (JCPDS card, No. 04-0783), which indicates that the silver nanoparticles are composed of pure crystalline silver [33].

Figure 1b shows the FTIR spectra of GICs, Ag-GICs, and Ag-EG. For GICs, there is a strong absorption band at 3430 cm^{-1}, which corresponded to the O–H stretching vibrations. It also exhibits bands around 1720 cm^{-1} due to the C=O stretching, 1630 cm^{-1} due to aromatic C=C, as well as bands due to carboxy C–O (1450 cm^{-1}), and a strong band at 1050 cm^{-1} attributed to C–O stretching vibrations. It has been reported previously that these groups are situated at the edges of the graphite nanosheets [34]. However, an obvious change of the absorption bands of the oxygenated functional groups was seen in the FT-IR spectrum of the Ag-GICs, and the peak at 1720 cm^{-1} corresponds to the C=O groups. This could be attributed to both the reduction of $NaBH_4$ and the existence of the AgNPs on the surface of GICs [33,35]. The oxygenated functional groups of Ag-EG was further decreased. The spectrum also presents a C=C peak at 1630 cm^{-1} corresponding to the remaining sp^2 character from the unoxidized graphitic domains. From the FT-IR spectra, it could be deduced that functional groups provide ideal nucleation sites for Ag nanoparticles; powerful interactions would occur between Ag nanoparticles and the un-reduced oxygen-containing groups on the surface of the GICs and that of the EG. Therefore, Ag nanoparticles can strongly attach to the exfoliated graphite surface [23].

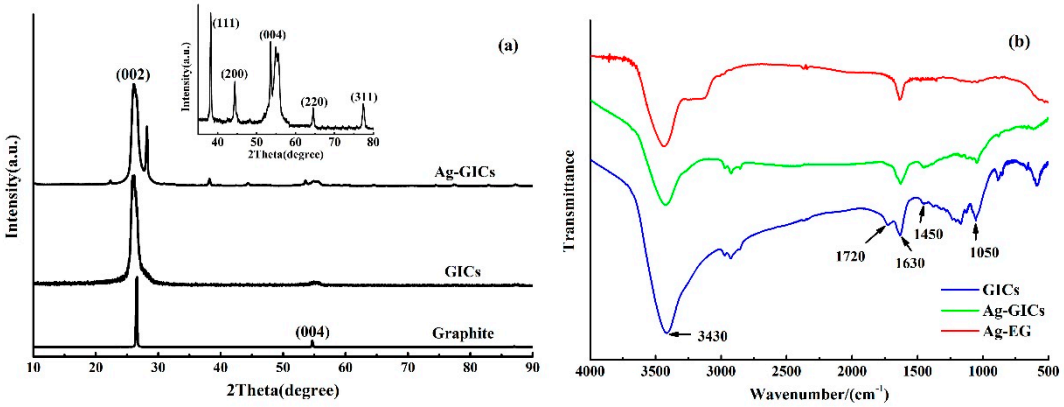

Figure 1. (**a**) X-ray diffraction (XRD) patterns of flake graphite, graphite intercalation compounds (GICs), and Ag-GICs, insert shows XRD patterns of Ag-GICs, the 2Theta from 35° to 80°; (**b**) FT-IR spectra of GICs, Ag-GICs, and Ag-EG.

3.2. Morphology Observation by SEM and TEM

Figure 2 shows SEM images of Ag nanoparticles-loaded EG. EG has a worm-like shape (Figure 2c). Due to its loose and porous character, the EG volume is hundreds times that of the GICs, which leads to the very low density of EG [36,37]. Only the spacing of the graphite layers (C axis) was expanded; thus the conductive characteristics of each EG sheet layer remains the same as graphite flakes by nature.

One GIC had been split into thousands of smaller pieces without separating completely, therefore there is plenty of pores in EG, shown in Figure 2d. In addition, some functional groups such

as hydroxyl, carboxyl, carbonyl groups existed on the surface and pores of the EG after acid and high temperature treatments, and they could promote the adsorption of polar molecule.

Figure 2e shows the distribution of Ag particles. Most particles have a diameter less than 10 nm, but there are some particles that appear larger size, which could be the result of aggregation of two or more particles together. The Ag particles size and quantity are influenced by the concentration of the $AgNO_3$ solution. With the increase of concentration, the Ag particles appeared in larger size, and there are more Ag particles decorated on the EG sheets [25].

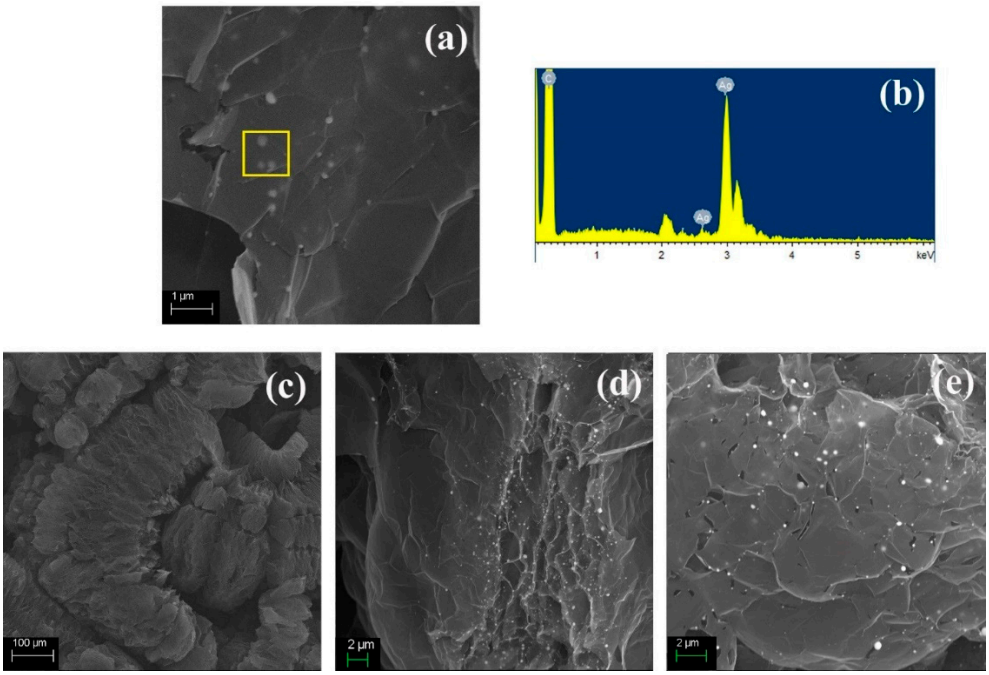

Figure 2. Scanning electron microscopy (SEM) images of Ag nanoparticles-loaded EG. (**a**) Ag nanoparticles synthesized on EG sheets; (**b**) the corresponding selected area energy dispersive spectrometer (EDS); (**c**) the worm-like shape of EG; (**d**) pores in EG; (**e**) defects on EG sheets where Ag nanoparticles grew on.

Figure 3 shows transmission electron microscopy (TEM) images of Ag nanoparticles-decorated exfoliated graphite. A low-magnification TEM micrograph (Figure 3a) presents plenty of wrinkles owing to the thin structure of the sheet. Uniform single-entity Ag nanoparticles embedded in the sheets after ultrasonication, revealing that there is a good inherent interfacial bonding in Ag and expansible graphite. The distribution of particles ranges in the diameter less than 10 nm (the average diameter of about 100 particles), the smaller particles are spherical in shape, whereas the larger nanoparticles are in an anomalous form. The presence of the bigger particles can be due to agglomeration of the two or more particles together. Ag nanoparticles loaded on EG comes near to the size of those loaded on GO sheets [23], but smaller than those loaded on ACFs [38,39]. Figure 3c clearly shows the interface between the sheet and Ag, indicating that Ag nanoparticles are well attached between the surfaces of the sheet. The measured lattice fringe spacing of 0.23 nm in these Ag nanoparticles corresponds to the (111) crystal plane.

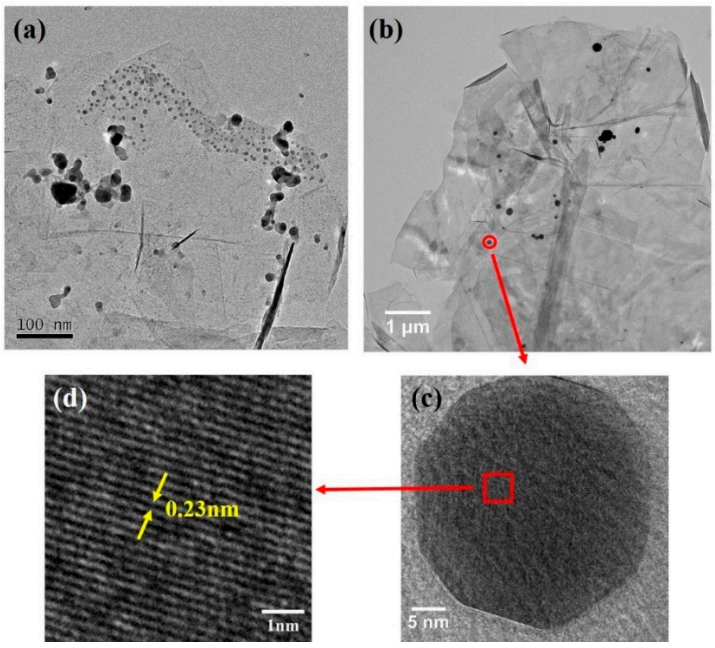

Figure 3. Transmission electron microscopy (TEM) images of Ag nanoparticles on the EG sheets, (**a**,**b**) Ag nanoparticles coating on the EG sheets after exfoliated through ultrasonication; (**c**) High-resolution transmission electron microscopy (HRTEM) with fringe spacing; (**d**) is an enlarged image of fringe spacing.

3.3. Pore Structure by Nitrogen Adsorption and Mercury Intrusion Porosimetry Measurement

The N_2 adsorption-desorption isotherms of EG and Ag-EG (Figure 4a) shows that both of the hysteresis loops of EG and Ag-EG were of similar type, indicating slit pores and laminated structure. The BET surface area of Ag-EG was calculated to be 56.9 $m^2 \cdot g^{-1}$, with an increase of 36.5% in comparison to EG. The pore size distribution measured by mercury intrusion porosimetry (Figure 4b) shows that EG has abundant macropores with diameter from 20 to 200 μm. After Ag loading, the total pore volume decreased from 40.33 $mL \cdot g^{-1}$ of EG to 27.77 $mL \cdot g^{-1}$ of Ag-EG. The N_2 adsorption-desorption isotherms and mercury intrusion porosimetry results indicated that the silver nanoparticles loading significantly decreased the porosity at the micron scales, but slightly increased the surface area of EG. Thus, the AgNPs-loaded EG still retained the excellent adsorption capacity of EG, which is useful for bacteria adsorption and inactivation.

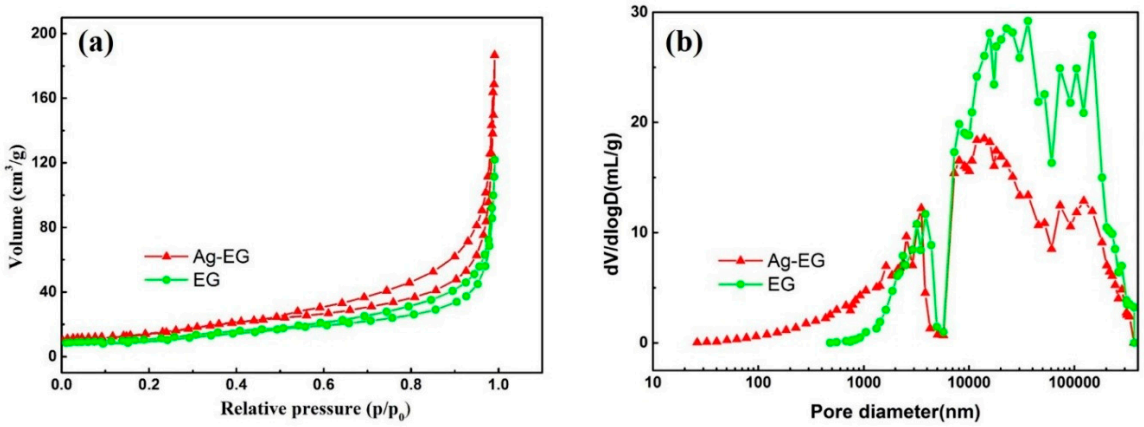

Figure 4. (**a**) N_2 adsorption-desorption isotherms; (**b**) the pore size distribution measured by mercury intrusion porosimetry measurement.

3.4. Inhibition Ring Test and Anti-Adhesion Effect of Bacteria

We synthesized silver nanoparticles-loaded exfoliated graphite with different Ag loading by using different concentrations of $AgNO_3$. The silver content of samples was analyzed by ICP-AES. The results are summarized in Table 1.

Table 1. Sliver content of Ag-EG synthesized with different concentrations of $AgNO_3$.

Concentrations of $AgNO_3/10^{-3}$ mol·dm^{-3}	0.3125	0.625	1.25	2.5	5	20	80
Sliver content/%	0.071	0.16	0.38	0.73	1.26	3.75	8.24

The anti-bacterial activity of the Ag-EG against Gram negative bacteria *P. aeruginosa* and Gram positive bacteria *S. aureus* was evaluated using the zone of inhibition method. In nutrient agar plates containing different Ag-EG that were made into round pieces, there are four of the same round pieces on every plate to decrease errors. Figures 5 and 6 show that the expanded graphite without Ag nanoparticles did not show any antibacterial properties, while the others exhibited different antibacterial activities. The antimicrobial mechanism of silver nanoparticles is not completely understood. The most accepted mechanism is related to the fact that silver nanoparticles can release Ag^+ ions, which may affect the metabolic processes and the mechanism of cell division, causing serious problems in the membrane permeability, resulting in the death of the bacteria [40,41].

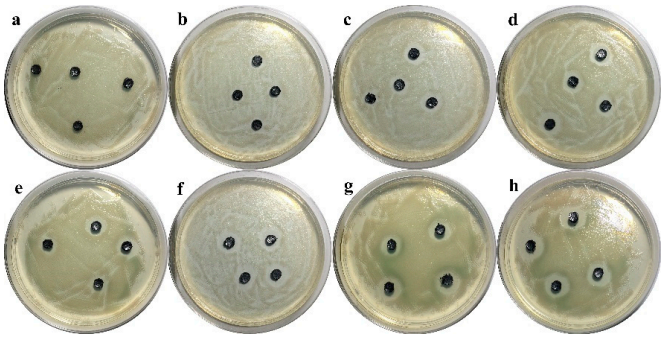

Figure 5. Inhibition zones of different contents of AgNPs with *P. aeruginosa*: (**a**), control (EG); (**b**–**h**), Ag-EG which was synthesized by 3.125×10^{-4} mol·dm^{-3} (9.4 ± 0.3 mm, n = 4), 6.25×10^{-4} mol·dm^{-3} (10.8 ± 0.8 mm, n = 4), 1.25×10^{-3} mol·dm^{-3} (12.3 ± 0.4 mm, n = 4), 2.5×10^{-3} mol·dm^{-3} (13.1 ± 0.8 mm, n = 4), 5×10^{-3} mol·dm^{-3} (14.9 ± 0.4 mm, n = 4), 2×10^{-2} mol·dm^{-3} (15.1 ± 0.9 mm, n = 4), 8×10^{-2} mol·dm^{-3} (15.3 ± 0.4 mm, n = 4) $AgNO_3$ solution.

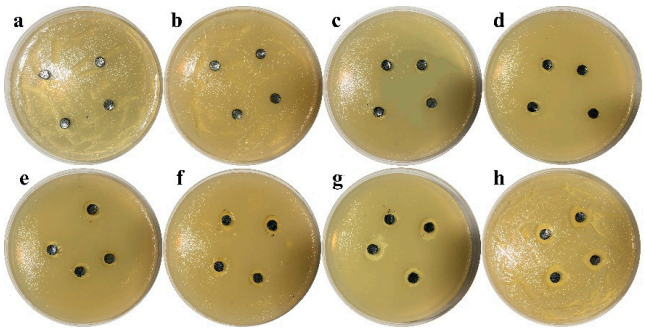

Figure 6. Inhibition zone of different content of AgNPs with *S. aureus*: (**a**), control (EG); (**b**–**h**), Ag-EG which was synthesized by 3.125×10^{-4} mol·dm^{-3} (7.2 ± 0.5 mm, n = 4), 6.25×10^{-4} mol·dm^{-3} (9.4 ± 0.3 mm, n = 4), 1.25×10^{-3} mol·dm^{-3} (9.8 ± 0.6 mm, n = 4), 2.5×10^{-3} mol·dm^{-3} (10.7 ± 0.5 mm, n = 4), 5×10^{-3} mol·dm^{-3} (12.5 ± 0.3 mm, n = 4), 2×10^{-2} mol·dm^{-3} (13.9 ± 0.7 mm, n = 4), 8×10^{-2} mol·dm^{-3} (14.4 ± 0.3 mm, n = 4) $AgNO_3$ solution.

Figure 7 shows the influence of silver loading on the inhibition zones. Both two curves showed the diameters of the inhibition zones increased with the increasing Ag content when the Ag content was less than 1.26% for *P. aeruginosa*, 3.75% for *S. aureus*, but almost did not change when the content continued to increase. It was also observed that *P. aeruginosa* was comparatively more sensitive to the Ag-EG and produced larger growth inhibition zones. In high content, the agglomeration of Ag nanoparticles meant that it was harder to release Ag^+. The experiment showed that Ag-EG has anti-bacterial activity against *P. aeruginosa* and *S. aureus*, and the Ag content is much less than that of Ag-GO [33,42].

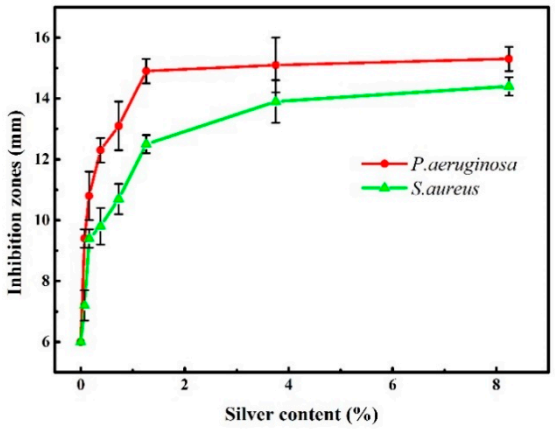

Figure 7. The relationship between inhibition zones and silver content. The error bars represent the standard deviation of the experiments performed in quadruplicate (n = 4).

Figure 8 shows the adhesion of *P. aeruginosa* and *S. aureus* on the surface of the EG and Ag-EG after incubating with washed bacteria for 2 h and 12 h. There were no bacterial colonies around Ag-EG round pieces after either incubating time. In contrast, some bacterial colonies grew around EG round pieces. This phenomenon was observed in both *P. aeruginosa* and *S. aureus*. Hence, the Ag-EG material exhibited significant improvement in the property of anti-bacterial adhesion. This experiment demonstrated that Ag-EG material can be used in a variety of large scale industrial applications that require materials with long term antibacterial and anti-adhesion properties.

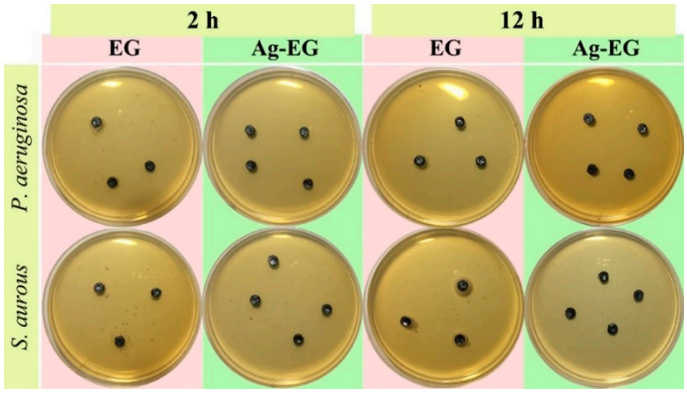

Figure 8. Bacterial adhesion on the surface of the EG and Ag-EG after incubating with washed bacteria for 2 h and 12 h.

4. Conclusions

Silver nanoparticles-loaded exfoliated graphite composite was prepared by impregnation reduction, followed by an thermal expansion method. AgNPs were highly dispersed and strongly

attached to the edges and the defects of the EG sheets. The sliver content and the size of AgNPs were influenced by $AgNO_3$ concentration. The loading of silver nanoparticles significantly decreased the porosity at the micron scale, but slightly increased the surface area of EG. An inhibition zone test and anti-adhesion test against *P. aeruginosa* and *S. aureus* showed Ag-EG composite material has anti-bacterial activity and anti-adhesion properties. The anti-bacterial activity increased with the increasing Ag loading up to 1.26% for *P. aeruginosa* and 3.75% for *S. aureus*, and then remained constant. The Ag-EG composites could be used in a variety of industrial applications that require an antibacterial effect, such as surgical dressing and effluent treatment.

Author Contributions: Shiyu Hou and Zheng-Hong Huang conceived and designed the experiments; Shiyu Hou performed the experiments; Shiyu Hou, Jihui Li, Liqiang Ma, Wanci Shen, Feiyu Kang and Zheng-Hong Huang analyzed the data; Xiaochuan Huang and Xiaomao Wang contributed reagents/materials/analysis tools; Shiyu Hou and Zheng-Hong Huang wrote the paper.

Conflicts of Interest: The authors declare no conflict of interest.

References

1. Tomacheski, D.; Pittol, M.; Simoes, D.N.; Ribeiro, V.F. Effect of natural ageing on surface of silver loaded TPE and its influence in antimicrobial efficacy. *Appl. Surf. Sci.* **2017**, *405*, 137–145. [CrossRef]
2. Pak, Z.H.; Abbaspour, H.; Karimi, N.; Fattahi, A. Eco-friendly synthesis and antimicrobial activity of silver nanoparticles using dracocephalum moldavica seed extract. *Appl. Sci.* **2016**, *6*, 69. [CrossRef]
3. Nguyen, H.L.; Jo, Y.K.; Cha, M.; Cha, Y.J.; Yoon, D.K.; Sanandiya, N.D.; Prajatelistia, E.; Oh, D.X.; Hwang, D.S. Mussel-inspired anisotropic nanocellulose and silver nanoparticle composite with improved mechanical properties, electrical conductivity and antibacterial activity. *Polymers* **2016**, *8*, 102. [CrossRef]
4. Porcaro, F.; Carlini, L.; Ugolini, A.; Visaggio, D.; Visca, P.; Fratoddi, I.; Venditti, I.; Meneghini, C.; Simonelli, L. Synthesis and structural characterization of silver nanoparticles stabilized with 3-Mercapto-1-Propansulfonate and 1-Thioglucose mixed thiols for antibacterial applications. *Materials* **2016**, *9*, 1028. [CrossRef] [PubMed]
5. Aruguete, D.M.; Kim, B.; Hochella, M.F.; Ma, Y.J.; Cheng, Y.W.; Hoegh, A.; Liu, J.; Pruden, A. Antimicrobial nanotechnology: Its potential for the effective management of microbial drug resistance and implications for research needs in microbial nanotoxicology. *Environ. Sci. Process. Impacts* **2013**, *15*, 93–102. [CrossRef] [PubMed]
6. Rieger, K.A.; Cho, H.J.; Yeung, H.F.; Fan, W.; Schiffman, J.D. Antimicrobial activity of silver ions released from zeolites immobilized on cellulose nanofiber mats. *ACS Appl. Mater. Interfaces* **2016**, *8*, 3032–3040. [CrossRef] [PubMed]
7. Rocks, L.; Faulds, K.; Graham, D. Rationally designed SERS active silica coated silver nanoparticles. *Chem. Commun.* **2011**, *47*, 12886. [CrossRef] [PubMed]
8. Uzayisenga, V.; Lin, X.D.; Li, L.M.; Anema, J.R.; Yang, Z.L.; Huang, Y.F.; Lin, H.X.; Li, S.B.; Li, J.F.; Tian, Z.Q. Synthesis, characterization, and 3D-FDTD simulation of $Ag@SiO_2$ nanoparticles for shell-isolated nanoparticle-enhanced raman spectroscopy. *Langmuir* **2012**, *28*, 9140–9146. [CrossRef] [PubMed]
9. Sotiriou, G.A.; Teleki, A.; Camenzind, A.; Krumeich, F.; Meyer, A.; Panke, S.; Pratsinis, S.E. Nanosilver on nanostructured silica: Antibacterial activity and Ag surface area. *Chem. Eng. J.* **2011**, *170*, 547–554. [CrossRef] [PubMed]
10. Xu, P.; Liang, J.; Cao, X.; Tang, J.; Gao, J.; Wang, L.; Shao, W.; Gao, Q.; Teng, Z. Facile synthesis of monodisperse of hollow mesoporous SiO2 nanoparticles and in-situ growth of Ag nanoparticles for antibacterial. *J. Colloid Interface Sci.* **2016**, *474*, 114–118. [CrossRef] [PubMed]
11. Zhao, L.Z.; Wang, H.R.; Huo, K.F.; Cui, L.Y.; Zhang, W.R.; Ni, H.W.; Zhang, Y.M.; Wu, Z.F.; Chu, P.K. Antibacterial nano-structured titania coating incorporated with silver nanoparticles. *Biomaterials* **2011**, *32*, 5706–5716. [CrossRef] [PubMed]
12. Bhatnagar, A.; Hogland, W.; Marques, M.; Sillanpaa, M. An overview of the modification methods of activated carbon for its water treatment applications. *Chem. Eng. J.* **2013**, *219*, 499–511. [CrossRef]
13. Tang, C.L.; Sun, W.; Yan, W. Green and facile fabrication of silver nanoparticles loaded activated carbon fibers with long-lasting antibacterial activity. *RSC Adv.* **2014**, *4*, 523–530. [CrossRef]

14. Chingombe, P.; Saha, B.; Wakeman, R.J. Sorption of atrazine on conventional and surface modified activated carbons. *J. Colloid Interface Sci.* **2006**, *302*, 408–416. [CrossRef] [PubMed]
15. Tang, C.; Hu, D.; Cao, Q.; Yan, W.; Xing, B. Silver nanoparticles-loaded activated carbon fibers using chitosan as binding agent: Preparation, mechanism, and their antibacterial activity. *Appl. Surf. Sci.* **2017**, *394*, 457–465. [CrossRef]
16. Zhang, S.T.; Wu, D.C.; Wan, L.; Tan, H.B.; Fu, R.W. Adsorption and antibacterial activity of silver-dispersed carbon aerogels. *J. Appl. Polym. Sci.* **2006**, *102*, 1030–1037. [CrossRef]
17. Kazmi, S.J.; Shehzad, M.A.; Mehmood, S.; Yasar, M.; Naeem, A.; Bhatti, A.S. Effect of varied Ag nanoparticles functionalized CNTs on its anti-bacterial activity against *E. coli*. *Sens. Actuator A Phys.* **2014**, *216*, 287–294. [CrossRef]
18. Khare, P.; Ramkumar, J.; Verma, N. Control of bacterial growth in water using novel laser-ablated metal–carbon–polymer nanocomposite-based microchannels. *Chem. Eng. J.* **2015**, *276*, 65–74. [CrossRef]
19. Sun, X.F.; Qin, J.; Xia, P.F.; Guo, B.B.; Yang, C.M.; Song, C.; Wang, S.G. Graphene oxide-silver nanoparticle membrane for biofouling control and water purification. *Chem. Eng. J.* **2015**, *281*, 53–59. [CrossRef]
20. Chae, H.R.; Lee, J.; Lee, C.H.; Kim, I.C.; Park, P.K. Graphene oxide-embedded thin-film composite reverse osmosis membrane with high flux, anti-biofouling, and chlorine resistance. *J. Membr. Sci.* **2015**, *483*, 128–135. [CrossRef]
21. Zhang, H.Z.; Zhang, C.; Zeng, G.M.; Gong, J.L.; Ou, X.M.; Huan, S.Y. Easily separated silver nanoparticle-decorated magnetic graphene oxide: Synthesis and high antibacterial activity. *J. Colloid Interface Sci.* **2016**, *471*, 94–102. [CrossRef] [PubMed]
22. Gerasymchuk, Y.; Lukowiak, A.; Wedzynska, A.; Kedziora, A.; Bugla-Ploskonska, G.; Piatek, D.; Bachanek, T.; Chernii, V.; Tomachynski, L.; Strek, W. New photosensitive nanometric graphite oxide composites as antimicrobial material with prolonged action. *J. Inorg. Biochem.* **2016**, *159*, 142–148. [CrossRef] [PubMed]
23. De Faria, A.F.; Martinez, D.S.T.; Meira, S.M.M.; de Moraes, A.C.M.; Brandelli, A.; Souza, A.G.; Alves, O.L. Anti-adhesion and antibacterial activity of silver nanoparticles supported on graphene oxide sheets. *Colloids Surf. B Biointerfaces* **2014**, *113*, 115–124. [CrossRef] [PubMed]
24. Liu, L.; Liu, J.C.; Wang, Y.J.; Yan, X.L.; Sun, D.D. Facile synthesis of monodispersed silver nanoparticles on graphene oxide sheets with enhanced antibacterial activity. *New J. Chem.* **2011**, *35*, 1418–1423. [CrossRef]
25. Das, M.R.; Sarma, R.K.; Saikia, R.; Kale, V.S.; Shelke, M.V.; Sengupta, P. Synthesis of silver nanoparticles in an aqueous suspension of graphene oxide sheets and its antimicrobial activity. *Colloids Surf. B Biointerfaces* **2011**, *83*, 16–22. [CrossRef] [PubMed]
26. Zacharia, R.; Ulbricht, H.; Hertel, T. Interlayer cohesive energy of graphite from thermal desorption of polyaromatic hydrocarbons. *Phys. Rev. B* **2004**, *69*. [CrossRef]
27. Wang, H.L.; Zhao, Y.; Ma, L.K.; Fan, P.H.; Xu, C.B.; Jiao, C.L.; Lin, A.J. Preparation of composite modified expanded graphite and its adsorption on acid brilliant blue dye. *Chem. J. Chin. Univ. Chin.* **2016**, *37*, 335–341.
28. Ntsendwana, B.; Sampath, S.; Mamba, B.B.; Oluwafemi, O.S.; Arotiba, O.A. Photoelectrochemical degradation of eosin yellowish dye on exfoliated graphite-ZnO nanocomposite electrode. *J. Mater. Sci. Mater. Electron.* **2016**, *27*, 592–598. [CrossRef]
29. Lin, Y.H.; Lin, J.H.; Wang, S.H.; Ko, T.H.; Tseng, G.C. Evaluation of silver-containing activated carbon fiber for wound healing study: In vitro and in vivo. *J. Biomed. Mater. Res. B* **2012**, *100*, 2288–2296. [CrossRef] [PubMed]
30. Singh, S.; Ashfaq, M.; Singh, R.K.; Joshi, H.C.; Srivastava, A.; Sharma, A.; Verma, N. Preparation of surfactant-mediated silver and copper nanoparticles dispersed in hierarchical carbon micro-nanofibers for antibacterial applications. *New Biotechnol.* **2013**, *30*, 656–665. [CrossRef] [PubMed]
31. Ma, C.F.; Gao, Q.; Xia, K.S.; Huang, Z.Y.; Han, B.; Zhou, C.G. Three-dimensionally porous graphene: A high-performance adsorbent for removal of albumin-bonded bilirubin. *Colloids Surf. B Biointerfaces* **2017**, *149*, 146–153. [CrossRef] [PubMed]
32. Malas, A.; Das, C.K. Influence of modified graphite flakes on the physical, thermo-mechanical and barrier properties of butyl rubber. *J. Alloy. Compd.* **2017**, *699*, 38–46. [CrossRef]
33. Vatanpour, V.; Shockravi, A.; Zarrabi, H.; Nikjavan, Z.; Javadi, A. Fabrication and characterization of anti-fouling and anti-bacterial Ag-loaded graphene oxide/polyethersulfone mixed matrix membrane. *J. Ind. Eng. Chem.* **2015**, *30*, 342–352. [CrossRef]

34. Park, S.; An, J.H.; Jung, I.W.; Piner, R.D.; An, S.J.; Li, X.S.; Velamakanni, A.; Ruoff, R.S. Colloidal suspensions of highly reduced graphene oxide in a wide variety of organic solvents. *Nano Lett.* **2009**, *9*, 1593–1597. [CrossRef] [PubMed]
35. Marcano, D.C.; Kosynkin, D.V.; Berlin, J.M.; Sinitskii, A.; Sun, Z.Z.; Slesarev, A.; Alemany, L.B.; Lu, W.; Tour, J.M. Improved synthesis of graphene oxide. *ACS Nano* **2010**, *4*, 4806–4814. [CrossRef] [PubMed]
36. Chen, G.H.; Wu, D.J.; Weng, W.U.; Wu, C.L. Exfoliation of graphite flake and its nanocomposites. *Carbon* **2003**, *41*, 619–621. [CrossRef]
37. Kang, F.Y.; Zheng, Y.P.; Wang, H.N.; Nishi, Y.; Inagaki, M. Effect of preparation conditions on the characteristics of exfoliated graphite. *Carbon* **2002**, *40*, 1575–1581. [CrossRef]
38. Xue, C.-H.; Chen, J.; Yin, W.; Jia, S.T.; Ma, J.Z. Superhydrophobic conductive textiles with antibacterial property by coating fibers with silver nanoparticles. *Appl. Surf. Sci.* **2012**, *258*, 2468–2472. [CrossRef]
39. Su, C.-I.; Peng, C.-C.; Lu, Y.-C. Silver-supporting modification of viscose rayon-based activated carbon fabrics. *Text. Res. J.* **2009**, *79*, 1486–1501. [CrossRef]
40. Feng, Q.; Wu, J.; Chen, G.; Cui, F.; Kim, T.; Kim, J. A mechanistic study of the antibacterial effect of silver ions on Escherichia coli and Staphylococcus aureus. *J. Biomed. Mater. Res.* **2000**, *52*, 662–668. [CrossRef]
41. Dakal, T.C.; Kumar, A.; Majumdar, R.S.; Yadav, V. Mechanistic basis of antimicrobial actions of silver nanoparticles. *Front. Microbiol.* **2016**, *7*. [CrossRef] [PubMed]
42. Zhang, D.; Liu, X.; Wang, X. Green synthesis of graphene oxide sheets decorated by silver nanoprisms and their anti-bacterial properties. *J. Inorg. Biochem.* **2011**, *105*, 1181–1186. [CrossRef] [PubMed]